Published in final edited form as:
Ann Neurol. 2008 July ; 64(1): 71–87. doi:10.1002/ana.21408.

Dok-7 Myasthenia: Phenotypic and Molecular Genetic Studies in 16 Patients

Duygu Selcen, MD[1], **Margherita Milone, MD, PhD**[1], **Xin-Ming Shen, PhD**[1], **C. Michel Harper, MD**[1], **Anthony A. Stans, MD**[2], **Eric D. Wieben, PhD**[3], and **Andrew G. Engel, MD**[1]

1 *Department of Neurology and Neuromuscular Research Laboratory, Mayo Clinic, Rochester, MN*

2 *Department of Orthopedic Surgery, Mayo Clinic, Rochester, MN*

3 *Department of Biochemistry and Molecular Biology, Mayo Clinic, Rochester, MN*

Abstract

Objective—Detailed analysis of phenotypic and molecular genetic aspects of Dok-7 myasthenia in 16 patients.

Methods—We assessed our patients by clinical and electromyographic studies, by intercostal muscle biopsies for in vitro microelectrode analysis of neuromuscular transmission and quantitative electron microscopy EM of 409 end plates (EPs), and by mutation analysis, and expression studies of the mutants.

Results—The clinical spectrum varied from mild static limb-girdle weakness to severe generalized progressive disease. The synaptic contacts were single or multiple, and some, but not all, were small. In vitro microelectrode studies indicated variable decreases of the number of released quanta and of the synaptic response to acetylcholine; acetylcholine receptor (AChR) channel kinetics were normal. EM analysis demonstrated widespread and previously unrecognized destruction and remodeling of the EPs. Each patient carries 2 or more heteroallelic mutations: 11 in genomic DNA, 7 of which are novel; and 6 identifiable only in complementary DNA or cloned complementary DNA, 3 of which are novel. The pathogenicity of the mutations was confirmed by expression studies. Although the functions of Dok-7 include AChR β-subunit phosphorylation and maintaining AChR site density, patient EPs showed normal AChR β-subunit phosphorylation, and the AChR density on the remaining junctional folds appeared normal.

Interpretation—First, the clinical features of Dok-7 myasthenia are highly variable. Second, some mutations are complex and identifiable only in cloned complementary DNA. Third, Dok-7 is essential for maintaining not only the size but also the structural integrity of the EP. Fourth, the profound structural alterations at the EPs likely contribute importantly to the reduced safety margin of neuromuscular transmission.

Congenital myasthenic syndromes (CMS) are heterogeneous disorders in which the safety margin of neuromuscular transmission is compromised by one or more specific mechanisms. Between 1995 and 2005, defects in seven end-plate (EP)–associated proteins encoded by 10 different genes have been identified as molecular targets of the CMS.[1] In 2006, Okada and coworkers identified Dok-7 as a muscle-intrinsic activator of MuSK required for synaptogenesis.[2] Dok-7 harbors N-terminal pleckstrin homology (PH) and phosphotyrosine-

Address correspondence to Dr Engel, Department of Neurology, Mayo Clinic, Rochester, MN 55905. E-mail: age@mayo.edu.

Note Added in Proof

Monoallele mutation analysis by the Conversion technology[39] revealed absence of exons 3-6 in one allele in genomic DNA of *DOK7* in Patient 9.

binding (PTB) domains, and is strongly expressed at the postsynaptic region of skeletal muscle and in heart. Subsequently, mutations in *DOK7* were shown to cause a CMS that preferentially involved proximal limb muscles.[3–5] The majority of patients were heterozygous or homozygous for a 1124_1127dupTGCC mutation. Only this mutation was functionally characterized, and in two patients only a single mutation was detected.[3] Studies in six patients eventually shown to carry *DOK7* mutations demonstrated small EPs and simplified junctional folds, but the counts of the acetylcholine receptor (AChR) per EP were deemed appropriate for size of the EPs.[6] The amplitude of the synaptic response to acetylcholine (ACh), reflected by the amplitude of the miniature EP potential ($MEPP_A$) and EP potential (EPP_A), and the number of quanta released by nerve impulse *(m)* were reduced, whereas the amplitude of the miniature EP current ($MEPC_A$) was reported as normal. The impaired safety margin of neuromuscular transmission was attributed to the reduced EPP_A.[6]

This article describes clinical features of 16 unrelated CMS patients with Dok-7 myasthenia. In 14 of these patients, we analyze parameters of neuromuscular transmission in vitro and examine 613 EP regions of 409 EPs by quantitative electron microscopy. We find that the structural changes and the electrophysiological alterations are more variable than previously reported. We identify mutations in DNA or complementary DNA (cDNA) in each patient, and evaluate most of these mutations by expression studies.

Patients and Methods

Patients

Sixteen patients, 8 men and 8 women, presently 5 to 50 years of age, were investigated. Each patient was initially examined, and four were reexamined 5 to 17 years later after their initial visit (AGE); additional follow-up information came from follow-up letters from referring physicians or patients regarding disease management. All human studies were in accord with guidelines of the institutional review board of the Mayo Clinic.

Morphological Studies

Intercostal muscle specimens intact from origin to insertion were obtained from Patients 1 to 14 and from control subjects without muscle disease undergoing thoracic surgery. AChR, demonstrated with rhodamine-labeled α-bungarotoxin (α-bgt), was colocalized in cryosections with acetylcholinesterase (AChE) using a monoclonal anti-AChE antibody,[7] and with the phosphorylated epitope of the AChR β subunit using a polyclonal goat antibody (pAChRβ1 [Tyr-390]; Santa Cruz Biotechnology, Santa Cruz, CA).

Dok-7 was colocalized with AChR or AChE in cryostat sections of patient and control EPs. Dok-7 was demonstrated with 2μg/ml polyclonal rabbit anti–human antibody raised against residues 210 to 498 of human Dok-7 (H-284; Santa Cruz Biotechnology) followed by fluorescein isothiocyanate–labeled donkey anti–rabbit IgG (1:300; Jackson ImmunoResearch Laboratories, West Grove, PA); AChR was visualized with rhodamine-labeled α-bgt, and AChE with a monoclonal anti-AChE antibody.[7] Sections were photographed using Zeiss Apotome optics (Zeiss, Thornwood, NY).

Synaptic contact regions were visualized by a cytochemical reaction for AChE[8] on glutaraldehyde-fixed teased single muscle fibers. EPs were localized for electron microscopy[9] and quantitatively analyzed[10] by established methods. Peroxidase-labeled α-bgt was used for the ultrastructural localization of AChR.[11] The number of AChRs per EP was measured with [^{125}I]α-bgt, as described elsewhere.[12]

In Vitro Electrophysiology Studies

$MEPP_A$, $MEPC_A$, EPP_A in presence of curare, and estimates of m[13,14] were obtained in Patients 1 to 14. EPP_A in absence of curare at a given EP was estimated from $m \times$ mean $MEPP_A$. Single-channel patch-clamp recordings from intercostal muscle EPs in the cell-attached mode[15] were obtained in seven patients.

Mutation Analysis

DNA was isolated from muscle and blood by standard methods. *DOK7* nucleotides (nt) were numbered according to the messenger RNA sequence (GenBank accession number NM_173660.3). We used nine polymerase chain reaction (PCR) primer pairs to amplify and directly sequence the seven exons and their flanking noncoding regions of *DOK7,* as well as nine and three primer pairs to amplify and sequence introns 2 and 3, respectively. PCR-amplified fragments were purified with shrimp alkaline phosphatase and exonuclease I (USB, Park Ridge, IL), and sequenced with an ABI3730xI DNA sequencer (Applied Biosystems, Foster City, CA) using fluorescently labeled dideoxy terminators. Allele-specific PCR was used to screen for mutations in patient families and unrelated healthy control subjects. To identify second mutations not found in genomic DNA, we isolated cDNA by reverse transcriptase PCR from EP-enriched intercostal muscles. To identify different transcripts, we cloned entire coding regions of mutant and wild-type *DOK7* cDNA into pZsGreen-N1 vector (Clontech, Palo Alto, CA). Plasmids were purified by the QIAprep Spin Miniprep and Hispeed Plasmid Maxi Kit (Qiagen, Chatsworth, CA), and directly sequenced.

Expression Studies

DOK7 cDNA was cloned into the cytomegalovirus-based expression vector tagged with an N-terminal FLAG epitope (pCMV-Tag2; Stratagene, La Jolla, CA). Human embryonic kidney fibroblasts (HEK 293T) and C2C12 cells were from the American Type Cell Culture Collection.

Mutant cDNA was cloned directly from patient cDNA except for cDNA that harbored the 1263insC, 1378insC, 596delT, and 601C>T mutations, which were engineered into wild-type pCMV-Tag2 using the QuikChange Site-Directed Mutagenesis Kit (Stratagene). Presence of each mutation and absence of unwanted mutations were confirmed by sequencing the entire insert.

HEK cells were cotransfected with mutant or wild-type FLAG-tagged *DOK7* cDNA together with pSV-β-galactosidase (Promega, Madison, WI) or human *MUSK* cDNA (Origene, Rockville, MD) using FuGene6 (Roche, Indianapolis, IN). The cells were extracted with radioimmunoprecipitation (RIPA) solution supplemented with protease inhibitors[2] and electrophoresed. The blots were immuno-stained to detect Dok-7, for tubulin to control for loading, and for β-galactosidase to control for transfection efficiency. MuSK was precipitated with rabbit anti-MuSK before electrophoresis, and the blots were stained with goat anti-MuSK and with anti-phosphotyrosine. After blocking with 5% non-fat milk or 1% bovine serum albumin, the blots were developed by the alkaline phosphatase method and quantitated using National Institutes of Health Image 1.63. The following antibodies were used: monoclonal anti-tubulin (Abcam, Cambridge, MA), monoclonal anti–β-galactosidase (Promega), monoclonal anti-FLAG (Sigma-Aldrich, St. Louis, MO), rabbit and goat anti-MuSK (Santa Cruz), and monoclonal anti-Ptyr clone 4G-10 (Upstate Biotechnology, Lake Placid, NY). Alkaline phosphatase–labeled antibodies were from Jackson ImmunoResearch Laboratories (West Grove, PA).

C2C12 cells were grown on polyornithine-coated (Sigma-Aldrich) and laminin-coated (Invitrogen, La Jolla, CA) wells.[16] Myoblasts were transfected with mutant or wild-type

DOK7. After differentiation for 6 to 7 days in 2% horse serum, the wells were incubated with Rh-bgt (Molecular Probes, Eugene, OR) in Dulbecco's minimum essential medium for 30 minutes at 37°C. After rinsing with phosphate-buffered saline, the cells were fixed with 2% paraformaldehyde, permeabilized with 0.1% (vol/vol) Triton X-100 (Sigma), blocked with 2% bovine serum albumin in phosphate-buffered saline, and then incubated with fluorescein isothiocyanate–conjugated anti-FLAG antibody (Sigma-Aldrich). The preparations were examined with a Zeiss Ax-iovert epifluorescence microscope using apotome optics, Axiovison 4.4 software, and 40× (1.3 numerical aperture) and 63× (1.4 NA) objectives. Transfected cells were recognized by their diffuse green fluorescence. AChR clusters ≥5μm were analyzed in transfected myotubes for axial length, numerical density, and shape. Cluster shapes were classified as simple or complex, the latter comprising C-shaped, perforated, or branching moieties.[16]

Results

Clinical Features

The age at onset of symptoms ranged from the first day of life to 5 years (mean, 1.6 years; median, 1 year). The clinical features are summarized in Table 1, presented in detail in Supplemental Table 1, and illustrated in Figure 1. The clinical course varied from mild static weakness limited to limb-girdle muscles to severe generalized progressive disease. All experienced short-term fatigability on exertion. As noted by others,[4,5] 10 patients experienced intermittent worsenings lasting from days to weeks. They differ from previous reports[4,5] in that three patients (Patients 7, 8, and 11) had been hypomotile in utero (see Discussion), and one (Patient 13) was unusual in having severe ptosis, facial weakness, and bulbar symptoms, but only slight shoulder muscle weakness (see Fig 1D). Seven patients had significant respiratory embarrassment. The overall course was progressive in 12 patients. Phenotypic features of Patient 9 were published previously.[17] Different therapeutic agents were tried in the 16 patients at different dosages and in different combinations (see Supplemental Table 1). Among 10 patients (Patients 1–5, 7, 8, 10, 11, and 14) initially treated with pyridostigmine, 6 patients (Patients 1, 3, 4, 8, 10, and 11) did not respond favorably, and the conditions of 3 patients (Patient 2, 5, 7) worsened; the condition of 1 patient (Patient 14) improved, but then worsened after the subsequent addition of 3,4-diaminopyridine. Three patients (Patients 9, 12, and 14) were treated with pyridostigmine plus 3,4-DAP; the condition of one patient (Patient 9) improved, but that of two patients (Patients 12 and 14) worsened. Four patients (Patients 8, 13, 15, and 16) were treated with 3,4-DAP alone; the conditions of two patients (Patients 8 and 15) improved, one patient (Patient 13) did not respond favorably, and the condition of 1 patient (Patient 16) worsened. Ephedrine alone improved the conditions of three patients (Patients 1, 2, and 6), and ephedrine plus with 3,4-DAP benefited two patients (Patients 4 and 7). Patient 3, who did not respond to pyridostigmine at age 6 years, showed an improvement with Albuterol in his twenties. Worsenings after exposure to cholinergic agents were noted within a few days to several weeks after start of exposure or dose escalation. Although the different dosage regimens and combination of agents are confounding variables, the above observations imply that cholinergic agent are of uncertain benefit or can worsen the symptoms of Dok-7 myasthenia.

Histochemistry

External intercostal muscle specimens in 14 patients showed type 1 fiber preponderance in 14, type 2 fiber atrophy in 8, isolated necrotic or regenerating fibers suggesting a myopathy in 4, pleomorphic decreases of oxidative enzyme activity in 12, and target formations suggesting denervation in 4 (see Supplementary Fig 1).

AChE-reactive synaptic contact areas on the muscle fibers were frequently punctate and small relative to fiber size (Fig 2B); others consisted of multiple small regions (see Figs 2D–F) linked by terminal nerve sprouts (see Fig 2D); still others were near normal or normal in size but lacked a normal pretzel configuration (see Figs 2A, C).

Because the degeneration of the postsynaptic junctional folds resembled that in the slow-channel syndrome,[18] and because these alterations are accompanied by Ca^{2+} accumulation in the junctional sarcoplasm,[19] we stained Dok-7 EPs with Alizarin red but detected no accumulation of Ca^{2+} in the junctional sarcoplasm.

Dok-7 was localized in EP-containing cryostat sections available from Patients 1, 4, 10, 12, and 14, non-weak control subjects, and patients with primary AChR deficiency caused by low-expressor mutations in AChR subunits. The sections from the Dok-7 patients and control subjects were also reacted for AChR, and the sections from patients with primary AChR deficiency were also immunostained for AChE.[7] EP expression of Dok-7 was readily detected in the control subjects, and in favorable sections, expressions of AChR and Dok-7 were topographically distinct (Figs 3A–C). Dok-7 expression was also detected in Patient 4, who is homozygous for the common 1124_1127dupTGCC mutation (see Figs 3G–I). Dok-7 expression was robust at EPs of mildly affected Patient 10 (see Figs 3J–L) and was markedly attenuated at EPs of severely affected Patient 12 (see Figs 3M–O). However, EP expression of Dok-7 was also strong in Patient 14, who was moderately severely affected (see Figs 3P–R), and was decreased in Patient 1, who was only mildly affected (see Figs 3D–F). Finally, decreased EP expression of Dok-7 was present in patients with primary EP AChR deficiency. In summary, we found no consistent correlation between the clinical state and EP expression of Dok-7, decreased EP expression of Dok-7 is not specific for Dok-7 myasthenia, and robust EP expression of Dok-7 does not preclude Dok-7 myasthenia.

End-Plate Ultrastructure

Electron micrographs of 613 EP regions of 409 EPs of Patients 1 to 14 were inspected for changes of EP conformation (Table 2). Some EP regions appeared normal (Fig 4A), but many displayed one or more of the following abnormalities: degeneration of junctional folds, frequently severe (Figs 4B, 5A, and 5B); partial occupancy by nerve terminal (Fig 6B) or absence of nerve terminal (see Figs 5A, B); highly simplified junctional folds (see Fig 4B); and degeneration of subsynaptic organelles (see Figs 5A, B). Some nerve terminals were partly (see Fig 6B) or completely encased by Schwann cell, and some were degenerating (see Fig 6B). Nerve sprouts appeared near degenerating or simplified EPs (see Figs 5A, B).

Consistent with the earlier observations, morphometric analysis of 340 EP regions showed a significantly reduced postsynaptic area. The length of the postsynaptic membrane, normalized for either the length of the primary synaptic cleft or the size of the postsynaptic area, was significantly reduced (Table 3). The AChR index (length of the AChR-reactive postsynaptic membrane normalized for the length of primary synaptic cleft) was also significantly decreased. However, the density and distribution of AChR on nondegenerate junctional folds was normal (see Figs 6A, B).

We detected no consistent correlation between conformational changes at the EPs and the clinical state, except that among five severely affected patients (Patients 5, 6, 7, 9, and 12), EPs of Patients 6, 7, and 9 displayed the greatest frequency of conformational changes.

In Vitro Electrophysiology Studies and Counts of Acetylcholine Receptors per End Plate

The overall means for $MEPP_A$, $MEPC_A$, and m were reduced, but the decrease in m did not reach statistical significance. However, EPP_A in absence of curare, predicted from $m \times$

$MEPP_A$, was significantly reduced. The number of AChRs per EP, estimated from the number of [^{125}I] binding sites per EP, was decreased to approximately 50% of normal (Table 4; see also Supplementary Figs 2 and 3). This decrease is attributed to the frequently small EPs and to focal loss of AChR from degenerating folds. However, for each parameter of neuromuscular transmission, the distributions of patient and control values overlapped (see Supplemental Figure 2).

The extensive degeneration of the junctional folds was similar to that observed in the slow-channel syndrome in which the AChR channel opens in markedly prolonged bursts, but patch-clamp recordings from EPs of seven patients indicated that the duration of channel opening bursts was close to normal (see Table 4), and that the AChR channels opened to a normal conductance of approximately 60 picosiemens.

We detected no correlation between the parameters of neuromuscular transmission and the clinical state except that three of five severely affected patients (Patients 6, 7, and 9) had the lowest $MEPP_A$ and predicted EPP_A values.

Mutation Analysis of DOK7

We identified 11 mutations in genomic DNA and 6 in cDNA isolated from EP-enriched muscle specimens (Table 5; Figs 7 and 8; and Supplementary Fig 4); 10 of these rearrangements are novel. Exon 3-4S appears in the National Cancer for Biotechnology Information (NCBI) database, and four of the observed rearrangements were reported previously,[3,5] but only the common 1124_1127dupTGCC mutation had been functionally characterized.[3]

Mutations in Genomic DNA

Among the mutations identified in genomic DNA, 7, including the common 1124_1127dupTGCC mutation, reside in exon 7, 2 reside in exon 5, a splice-site mutation appears in intron 1, and another in intron 3 (see Figs 7 and 8). Two mutations in Patient 13 are unusual: one is an insertion-deletion mutation in exon 7 (1139_41delinsA), and the other is a readthrough mutation (1513T>C) that extends the open reading frame by 182 missense residues.

Rearrangements in Complementary DNA

In Patients 2, 5, 9, and 10, a protracted search showed no second mutation in exons or at splice junctions. We therefore isolated messenger RNA from intercostal muscle specimens and searched for mutations in cDNA and cloned cDNA. In Patients 2 and 5, the second allele includes intron 1, predicting 23 missense residues followed by a stop codon (see Figs 7 and 8). Inclusion of intron 1 was not detected in 100 control cDNA samples. Interestingly, Patients 2 and 5 also carry a 15-nt deletion in intron 1 (54+14_28delGGGGGG-GGGGGGCGC), with one parent of each patient also carrying the 15-nt deletion. Deletion of 15 nt in intron 1 was not detected in genomic DNA of 100 healthy control subjects.

In Patient 9, analysis of 44 cDNA clones demonstrated that 91% show in-frame skipping (S) of exons 3 to 6 (Ex3-6S), and 9% harbor the 1001_1011dup mutation observed in genomic DNA (see Figs 7 and 8). Ex3-6S was not present in 100 control cDNA samples by allele-specific PCR.

In Patient 10, cDNA clones derived from messenger RNA by two separate reverse transcription yielded concordant results. Both sets of cDNA harbored six different transcripts. The combined frequencies in a total of 79 clones were Ex3-4S (17%); Ex2S (10%); Ex2-4S (11%); the common 1124_1127dupTGCC frameshift mutation (32%); both Ex2S and the common frame-shift mutation (9%); and no mutation (21%), consistent with cDNA mosaicism (see Figs 7 and

8). Ex2S was not detected in 100 healthy control subjects. We next searched by allele-specific PCR for Ex3-4S in cDNA isolated from 20 control muscles and found that 9 of 20 samples also showed Ex3-4S consistent with polymorphism. We next determined the frequency of the Ex3-4S in the three control samples that showed the highest level of expression in allele-specific PCR and found that only 1 of 12, 1 of 16, and 3 of 23 clones were Ex3-4S. In a further search for the cause of the multiple abnormal splice variants in Patient 10, we sequenced entire introns 2 and 3, and found no mutation that is likely to cause aberrant transcripts.

To further investigate the consequences of the splice-site mutations in Patients 8 and 12, we also cloned their cDNA. In Patient 8, 55-2A>C (IVS1-2A>C) results in recognition of a new splice site after the first 11 nt of exon 2, yielding 69 missense residues and a stop codon. Patient 12 harbors 331+1G>T (IVS3+1G>T) (see Figs 7 and 8). Examination of 42 cDNA clones shows Ex3-4S in 55%, Ex3S in 24%, Ex2-4S in 2%, the common frameshift mutation in 12%, and no mutation in 7%. Ex3S was not observed in 100 control cDNA samples by allele-specific PCR.

Expression Studies

Except for 1263delC, expression studies were performed to assess the pathogenicity of all mutations found in exons 5 and 7 of genomic DNA, and the 3 in-frame exon-skipping transcripts (Ex3S stemming from the 331+1G>T splice-site mutation, Ex3-4S, and Ex3-6S) detected in cDNA (see Fig 7).

Expression Studies in Human Embryonic Kidney Cells

HEK cells were transfected with wild-type *DOK7* cDNA, the three in-frame exon skipped (S) constructs (Ex3S, Ex 3-4S, Ex3-6S), and with the 1139_41de-linsA, 1263insC, 1513T>C, 1001_1011dup, 596delT, 601C>T, and 1378insC constructs. Densitometric analysis of immunoblots demonstrated significantly reduced expression of the Ex3S, Ex3-4S, 1513T>C, 596delT, and 601C>T mutants (Fig 9). To further investigate the consequences of these mutations, we examined their ability to phosphorylate MuSK. Only the in-frame Ex3S, Ex 3-4S, Ex3-6S transcripts that remove the PH, or both the PH and PTB, domains failed to phosphorylate MuSK (Fig 10). Phosphorylation of MuSK by the remaining *DOK7* mutants was not significantly different from that by wild type.

Expression Studies in C2C12 Myotubes

To assess the effects of identified mutations on the size, numerical density, and complexity of AChR clusters expressed by differentiated C2C12 myotubes, we transfected C2C12 myoblasts with FLAG-labeled constructs of 1001_1011dup, 1139_41delinsA, 1263insC, 1378insC, 1513T>C, and the previously characterized common 1124_1127dupTGCC mutation. The mutations expressed at the lowest level in HEK cells (596delT and 601C>T) and the exon-skipping mutations that failed to phosphorylate MuSK were not investigated in this system.

After 6 to 7 days in the differentiation medium, the axial length and density of the AChR clusters was significantly smaller in myotubes transfected with mutant than wild-type transcripts except for 1263insC (Fig 11; see Supplementary Table 2). Cluster complexity was evaluated by systematically traversing wells containing transfected myotubes and classifying the 200 first-encountered AChR clusters. For each construct, simple plaques were predominant; the more differentiated (complex) plaques comprising C-shaped, perforated, or branching moieties[16] accounted from 17 to 47% of the observed plaques. The frequency of the complex forms was significantly lower in myotubes transfected with mutant than wild-type transcripts (see Supplementary Fig 5).

Phosphorylation of the Acetylcholine Receptor β Subunit at Patient End Plates

An important function of activated MuSK is to phosphorylate the AChR β subunit, which, in turn, promotes anchoring and clustering of AChR.[20,21] We therefore immunostained intercostal muscle EPs of Patients 1, 4 to 7, and 9 to 12, and of 4 control subjects for the phosphorylated epitope of the AChR β subunit. We found that the reaction for this epitope at patient EPs was as intense as at control EPs (see Supplementary Fig 6). This was of particular interest in Patient 4 who carries the common 1124_1127dup mutation at homozygosity, because this mutation was reported to reduce AChR β subunit phosphorylation in myotubes.[3] In the remaining patients, presence on one allele of the similar common mutation must be sufficient to maintain AChR β-subunit phosphorylation when the second allele lacks the PH and PTB domains.

Discussion

Clinical Features

The clinical features of Dok-7 myasthenia do not distinguish it from some other forms of CMS. Mild involvement or sparing of the ocular or other cranial muscles can occur in the CMS caused by defects in EP AChE,[22] rapsyn,[23] and choline acetyltransferase. Cholinergic agonists also worsen the slow-channel syndrome,[24] but in this syndrome, the synaptic response to ACh is enhanced. In Dok-7 myasthenia, the adverse response to pyridostigmine is paradoxic because the synaptic response to ACh is decreased rather than increased.

Patients 7, 8, and 11 were hypomotile in utero. All three carry the common mutation; Patients 7 and 11 also carry a frameshift mutation (1263insC) in exon 7 that does not significantly reduce protein expression in HEK cells, and Patient 8 also carries a splice-site mutation in intron 1 that does not express in HEK cells (see Table 5; see also Figs 8 and 9). Patient 7 appeared normal in the neonatal period; she had delayed motor development and progressive weakness after the age of 5 years. Patient 8 had severe symptoms at birth and a progressive clinical course. Patient 11 presented with poor head control in infancy; he has a mild to moderately severe nonprogressive disease. Thus, uterine hypomotility does not reliably predict severe neonatal distress, reduced protein expression, or an unfavorable clinical course.

Although Dok-7 is strongly expressed in heart,[2] none of our patients had any cardiac symptoms. A possible reason for this could be that Dok-7 has a nonessential role in cardiac muscle or cardiac muscle harbors an alternate exon 7.

The changes in oxidative enzyme activity, including target formations in muscle fibers of 12 patients and the sparse necrotic or regenerating fibers in 4 patients, are of interest because they can confound the diagnosis, especially if careful electromyographic studies, including a search for a decremental response in the trapezius and facial muscles, are not performed. The changes in oxidative enzyme activity could be caused by functional denervation of the affected fibers. The cause of fiber necrosis is currently unclear.

End-Plate Studies

A previous study of six patients subsequently shown to have Dok-7 myasthenia showed single synaptic contacts for fiber size, decreased *m*, $MEPP_A$, and EPP_A, and simplified postsynaptic folds.[6] The decreased *m* was attributed to smallness of the synapse, and the decreased $MEPP_A$ to the reduced input resistance of the simplified folds. The $MEPC_A$, which is independent of input resistance, was not reduced, implying that the vesicular ACh content and the density and distribution of AChR on the folds were normal.

In this study, we found that the synaptic contacts can be multiple or single, that some are not small (see Fig 2), and that *m* is not appreciably reduced in most patients. The EM studies indicate ongoing destruction of existing EPs and attempts to form new EPs. Thus, simplification of folds at an EP can stem from their partial destruction (see Figs 4B and 5B), or from immaturity of newly formed postsynaptic regions, or is constitutive, or is due to a combination of these factors. However, that some EPs in each of 14 patients had normally developed folds (see Figs 4A and 6A) would argue against the simple folds being constitutive. The decreased $MEPP_A$ can be assigned to loss of AChR from degenerating folds, diffusional loss of ACh from widened synaptic spaces, and decreased input resistance of the remaining folds. The decreased $MEPC_A$, observed in some patients, is attributed to loss of AChR from degenerating folds and the altered geometry of the synaptic space.

Mutation Analysis

Each patient carries at least one pathogenic rearrangement on each allele, and 10 of the identified rearrangements are novel (see Fig 8). The identified rearrangements can be assumed to be pathogenic; four predict highly truncated transcripts (see Fig 8), and the remaining ones decrease one or more of the following: protein expression; MuSK phosphorylation in HEK cells; or the size, density, or complexity of the AChR clusters in myotubes.

The 15-nt deletion in intron 1 of Patients 2 and 5 was of special interest. This finding was not observed in genomic DNA of 100 control subjects. We considered the possibility that this deletion renders intron 1 to be too short to be recognized by the splicing machinery, but there are shorter introns in the human genome that are efficiently spliced.[25] The intron inclusion could also be caused by loss of G residues in the context of a less than optimal polypyrimidine tract.[26] The experimental testing of this hypothesis is beyond the scope of this report.

The Ex3-4S splice variant is of special interest. It accounts for 17 and 55% of cloned transcripts of Patients 10 and 12, respectively, but also appears at a low frequency in 9 of 20 control cDNA samples. Although by definition Ex3-4S is a polymorphism, it is potentially pathogenic because it deletes critical domains of the gene and abrogates the phosphorylation of MuSK; it thus differs from common null alleles in other genes with benign effects.[27,28] The functional role of a low copy number of the Ex3-4S transcript in some healthy subjects is not yet known.

In Patient 9, Ex3-6S in cDNA raises the question whether the DNA segment encompassing these exons is also absent from one allele in genomic DNA. Further investigation of this interesting question is beyond the scope of this communication. However, the fact remains that exon Ex3-6S at the cDNA level defines the second mutation in Patient 9. This mutation causes loss of critical coding domains of DOK7 (see Fig 7), and the Ex3-6S allele fails to phosphorylate MuSK (see Fig 10).

Genotype-phenotype correlations are hindered because each patient carries two, or even more than two, recessive rearrangements, and because the patients were observed at different points in course of an evolving disease. For example, Patient 8, who carries the common frameshift mutation and a canonical splice-site mutation, was mildly affected at the age of 8 years but was severely affected 6 years later. Patient 4, who is homozygous for the common mutation, has a slowly evolving disease and is moderately severely affected at the age of 55 years. A possible genotype-phenotype correlation exists in the least severely affected patient (Patient 10): He has only mild weakness at the age of 35 years, and 21% of his cloned cDNA is of the wild-type moiety.

Implications for the Pathogenesis of Dok-7 Myasthenia

Dok-7 is now firmly established as a muscle-intrinsic activator of MuSK[2] and is likely the previously postulated PTB-domain–containing cytoplasmic activator of MuSK.[29] In aneurally cultured C2C12 myotubes, activated MuSK signals downstream to induce clustering and anchoring of AChR via rapsyn[30] and phosphorylation of the AChR β subunit.[20,21] Knock-down of Dok-7 in C2C12 myotubes suppresses the phosphorylation and aggregation of AChR, [2] and forced expression of the common Dok-7 mutant decreases the length, complexity, and β-phosphorylation of the AChR clusters.[3]

In contrast with the extensive data on myotubes, little is known about the physiological roles of MuSK or Dok-7 at the innervated adult EP. Dok-7 mutations reduce EP size, but the AChR counts per EP are appropriate for EP size,[6] and AChR density on nonde-generate synaptic folds appears normal (see Figs 6A, B). It is now also known that prevention of AChR β phosphorylation in mice reduces synaptic size, AChR, and density, and alters the organization of the junctional folds.[31] However, the identified mutations in our patients do not abrogate the downstream effect of MuSK to cluster AChR via rapsyn or phosphorylate AChR. A likely explanation of this paradox is that each of our patients harbors at least one allele permissive of MuSK and AChR β phosphorylation. In addition, ShcD/Shc4, a recently discovered PTB-domain–containing second cytoplasmic binding partner of MuSK,[32] or agrin signaling via laminin[33] or β-catenin,[34] could contribute to concentrating AChRs at the EP.

Importantly, we find that defects in Dok-7 result in destruction and simplification of synaptic structures. The role of Dok-7 in maintaining normal EP structure is likely exerted via MuSK because conditional inactivation of MuSK in the mouse causes disassembly of the postsynaptic apparatus and disintegration of the EP.[35] Alternatively, defective Dok-7 function results in inappropriate activation of a proteolytic mechanism akin to that caused by enhanced ingress of Ca^{2+} into the postsynaptic region in the slow-channel syndrome.[19,36–38] Regardless of the exact molecular mechanism that results in the destructive changes at the EP, it is now clear that Dok-7 is crucial for maintaining not only the size but also the structural integrity of the innervated EP.

Supplementary Material

Refer to Web version on PubMed Central for supplementary material.

Acknowledgements

This study was supported by the NIHNINDS (K08, D.S.; NS6277, A.G.E.) and the Muscular Dystrophy Association (A.G.E.).

We thank Drs E. Trame, D. Talley, T. Heiman-Patterson, J. Wald, M. Bowen, R. Moxley, Z. Simmons, L. Morrison, M. Duren, C. Thornton, P. Humphreys, M. Melanson, R. Mantegazza, I. C. Verma, Y. Harati, and C. Gaston for patient referral.

References

1. Engel AG, Sine SM. Current understanding of congenital myasthenic syndromes. Curr Opin Pharmacol 2005;5:306–321.
2. Okada K, Inoue A, Okada M, et al. The muscle protein Dok-7 is essential for neuromuscular synaptogenesis. Science 2006;312:1802–1805. [PubMed: 16794080]
3. Beeson D, Higuchi O, Palace J, et al. Dok-7 mutations underlie a neuromuscular junction synaptopathy. Science 2006;313:1975–1978. [PubMed: 16917026]
4. Palace J, Lashley D, Newsom-Davis J, et al. Clinical features of the DOK7 neuromuscular junction synaptopathy. Brain 2007;130:1507–1515. [PubMed: 17452375]

5. Muller JS, Herczegfalvi A, Vilchez JJ, et al. Phenotypical spectrum of DOK7 mutations in congenital myasthenic syndromes. Brain 2007;130:1497–1506. [PubMed: 17439981]
6. Slater CR, Fawcett PRW, Walls TJ, et al. Pre- and postsynaptic abnormalities associated with impaired neuromuscular transmission in a group of patients with 'limb-girdle myasthenia. Brain 2006;127:2061–2076. [PubMed: 16870884]
7. Fambrough DM, Engel AG, Rosenberry TL. Acetylcholinesterase of human erythrocytes and neuromuscular junctions: homologies revealed by monoclonal antibodies. Proc Natl Acad Sci USA 1982;79:1078–1082. [PubMed: 6175961]
8. Gautron J. Cytochimie ultrastructurale des ace′vtylcholineste′rases. Microscopie 1974;21:259–264.
9. Engel, AG. The muscle biopsy. In: Engel, AG.; Franzini-Armstrong, C., editors. Myology. 3. New York: McGraw-Hill; 2004. p. 681-690.
10. Engel, AG. Quantitative morphological studies of muscle. In: Engel, AG.; Franzini-Armstrong, C., editors. Myology. 2. New York: McGraw-Hill; 1994. p. 1018-1045.
11. Engel AG, Lindstrom JM, Lambert EH, et al. Ultrastructural localization of the acetylcholine receptor in myasthenia gravis and in its experimental autoimmune model. Neurology 1977;27:307–315. [PubMed: 557772]
12. Engel AG. The investigation of congenital myasthenic syndromes. Ann N Y Acad Sci 1993;681:425–434. [PubMed: 7689310]
13. Engel AG, Nagel A, Walls TJ, et al. Congenital myasthenic syndromes. I. Deficiency and short open-time of the acetylcholine receptor. Muscle Nerve 1993;16:1284–1292. [PubMed: 8232383]
14. Uchitel O, Engel AG, Walls TJ, et al. Congenital myasthenic syndromes. II. A syndrome attributed to abnormal interaction of acetylcholine with its receptor. Muscle Nerve 1993;16:1293–1301. [PubMed: 8232384]
15. Milone M, Hutchinson DO, Engel AG. Patch-clamp analysis of the properties of acetylcholine receptor channels at the normal human endplate. Muscle Nerve 1994;17:1364–1369. [PubMed: 7526207]
16. Kummer TT, Misgeld T, Lichtman JW, et al. Nerve-independent formation of a topologically complex postsynaptic apparatus. J Cell Biol 2004;164:1077–1087. [PubMed: 15037598]
17. Milone M, Fukuda T, Shen X-M, et al. Novel congenital myasthenic syndromes associated with defects in quantal release. Neurology 2006;66:1223–1229. [PubMed: 16525123]
18. Engel AG, Lambert EH, Mulder DM, et al. A newly recognized congenital myasthenic syndrome attributed to a prolonged open time of the acetylcholine-induced ion channel. Ann Neurol 1982;11:553–569. [PubMed: 6287911]
19. Engel AG, Ohno K, Sine SM. Sleuthing molecular targets for neurological diseases at the neuromuscular junction. Nat Rev Neurosci 2003;4:339–352. [PubMed: 12728262]
20. Borges LS, Ferns M. Agrin-induced phosphorylation of the acetylcholine receptor regulates cytoskeletal anchoring and clustering. J Cell Biol 2001;153:1–12. [PubMed: 11285269]
21. Ferns M, Deiner M, Hall ZW. Agrin-induced acetylcholine receptor clustering in mammalian muscle requires tyrosine phosphorylation. J Cell Biol 1996;132:937–944. [PubMed: 8603924]
22. Hutchinson DO, Walls TJ, Nakano S, et al. Congenital end-plate acetylcholinesterase deficiency. Brain 1993;116:633–653. [PubMed: 8390325]
23. Burke G, Cossins J, Maxwell S, et al. Rapsyn mutations in hereditary myasthenia. Distinct early- and late-onset phenotypes. Neurology 2003;61:826– 828. [PubMed: 14504330]
24. Engel AG. The therapy of congenital myasthenic syndromes. Neurotherapeutics 2007;4:252–257. [PubMed: 17395135]
25. Ross TR, Grafham DV, Coffey AJ, et al. The DNA sequence of the human X chromosome. Nature 2005;434:325–337. [PubMed: 15772651]
26. McCullough AJ, Berget SM. G triplets located throughout a class of small vertebrate introns enforce intron borders and regulate splice site selection. Mol Cell Biol 1997;17:4562– 4571. [PubMed: 9234714]
27. Ioannidis JPA, Rosenberg PS, Goedert JJ, et al. Effects of CCR5-Delta32, CCR2– 64I, and SDF-1 3′ A alleles on HIV-1 disease progression: an international meta-analysis of individual-patient data. Ann Intern Med 2001;135:782–795. [PubMed: 11694103]

28. Yang N, MacArthur DG, Gulbin JP, et al. ACTN3 genotype is associated with human elite athletic performance. Am J Hum Genet 2003;73:627– 631. [PubMed: 12879365]
29. Zhou H, Glass DJ, Yancopoulos GD, et al. Distinct domains of MuSK mediate its abilities to induce and to associate with postsynaptic specializations. J Cell Biol 1999;146:1133–1146. [PubMed: 10477765]
30. Gautam M, Noakes PG, Mudd J, et al. Failure of postsynaptic specialization to develop at neuromuscular junctions of rapsyn-deficient mice. Nature 1995;377:232–236. [PubMed: 7675108]
31. Friese MB, Blagden CS, Burden SJ. Synaptic differentiation is defective in mice lacking acetylcholine receptor β-subunit tyrosine phosphorylation. Development 2007;134:4167–4176. [PubMed: 17959719]
32. Jones N, Hardy WR, Friese MB, et al. Analysis of a Shc family adaptor protein, ShcD/Shc4, that associates with muscle-specific protein kinase. Mol Cell Biol 2007;27:4759– 4773. [PubMed: 17452444]
33. Weston CA, Tressa G, Weeks BS, et al. Agrin and laminin induce acetylcholine receptor clustering by convergent, Rho GTPase-dependent signaling pathways. J Cell Sci 2006;120:868– 875. [PubMed: 17298982]
34. Zhang B, Luo S, Dong XP, et al. β-Catenin regulates acetylcholine receptor clustering in muscle cells through interaction with rapsyn. J Neurosci 2007;27:3968–3973. [PubMed: 17428970]
35. Hesser BA, Henschel O, Witzeman V. Synapse disassembly and formation of new synapses in postnatal muscle upon conditional inactivation of MuSK. Mol Cell Neurosci 2005;25:470– 479. [PubMed: 16337809]
36. Fucile S, Sucapane A, Grassi A, et al. The human adult subtype AChR channel has high Ca^{2+} permeability. J Physiol (London) 2006;573:35– 43. [PubMed: 16527851]
37. Di Castro A, Martinello K, Grassi F, et al. Pathogenic point mutations in a transmembrane domain of the ε subunit increase the Ca^{2+} permeability of the human endplate ACh receptor. J Physiol (London) 2007;579:671– 677. [PubMed: 17272341]
38. Groshong JS, Spencer MJ, Bhattacharyya BJ, et al. Calpain activation impairs neuromuscular transmission in a mouse model of the slow-channel myasthenic syndrome. J Clin Invest 2007;117:2903–2912. [PubMed: 17853947]
39. Highsmith WE, Meyer KJ, Marley VM, et al. Conversion technology for the seperation of material and paternal copies of any autosomal chromosome in somatic cell hybrids. Curr Protec Hum Genet 2007;55:3.6.1–3.6.38.

Fig 1.

Phenotypic variability of Dok-7 myasthenia. Patient 10 has mild weakness and atrophy of limb girdle muscles, and mild eyelid ptosis (A). Patient 6 has severe diffuse weakness and atrophy of limb and axial muscles (B). Patient 1 shows mild asymmetric ptosis with slight facial weakness (C). Patient 13 shows marked eyelid ptosis and severe facial weakness (D).

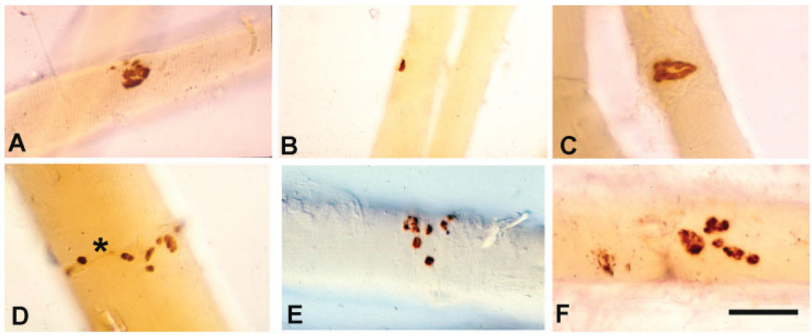

Fig 2.

Synaptic contact areas visualized with the cholinesterase reaction. Single small (B), multiple small (D–F), and perforated (A, C) contact areas were observed. Nerve sprouts are recognizable (D, asterisk) as faint brown lines connecting contact areas. Scale bar = 50μm.

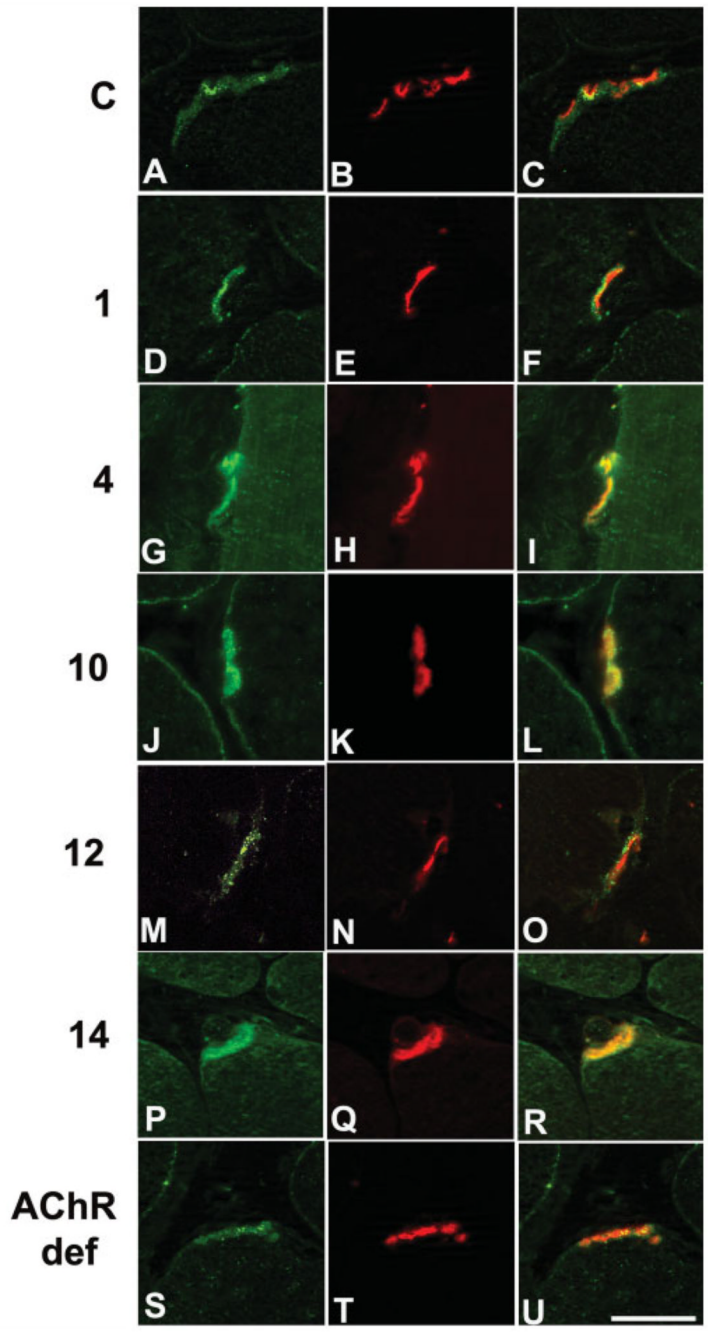

Fig 3.

End-plate (EP) localization of Dok-7 (green signal, left column), acetylcholine receptor (AChR; red signal, center column except T), acetylcholinesterase (AChE; T), and merge (right column) in control subject (C), in Patients 1, 4, 10, 12, and 14, and EP AChR deficiency caused by low-expressor AChR ε subunit mutations. Apotome optics, 0.43μm slice distance. Scale bar = 20μm.

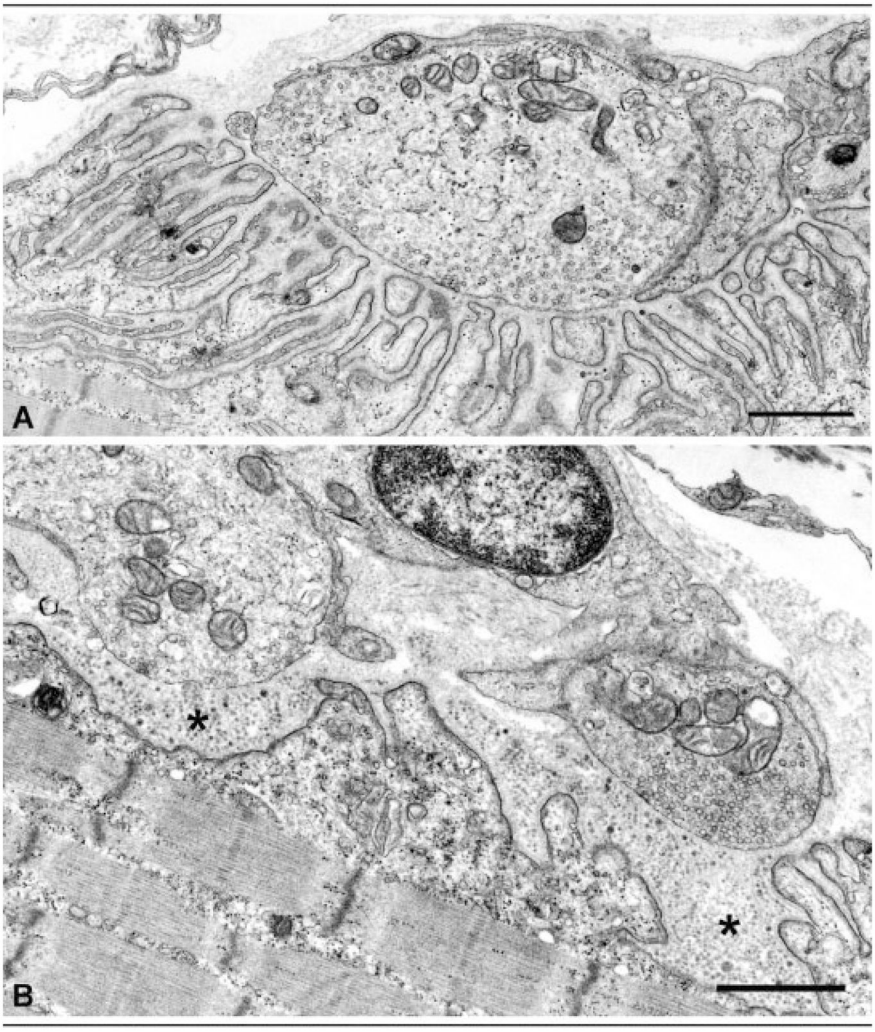

Fig 4.

Electron micrographs of normal (A) and degenerating (B) neuromuscular junction in same patient. (B) Most junctional folds are replaced by globular debris (asterisk), causing widening of the synaptic space. This predicts a decreased synaptic response to acetylcholine (ACh) caused by loss of acetylcholine receptor (AChR) from tips of the destroyed folds, loss of ACh by diffusion from the widened synaptic space, and decreased input resistance of the remaining simple folds. Scale bars = 1μm.

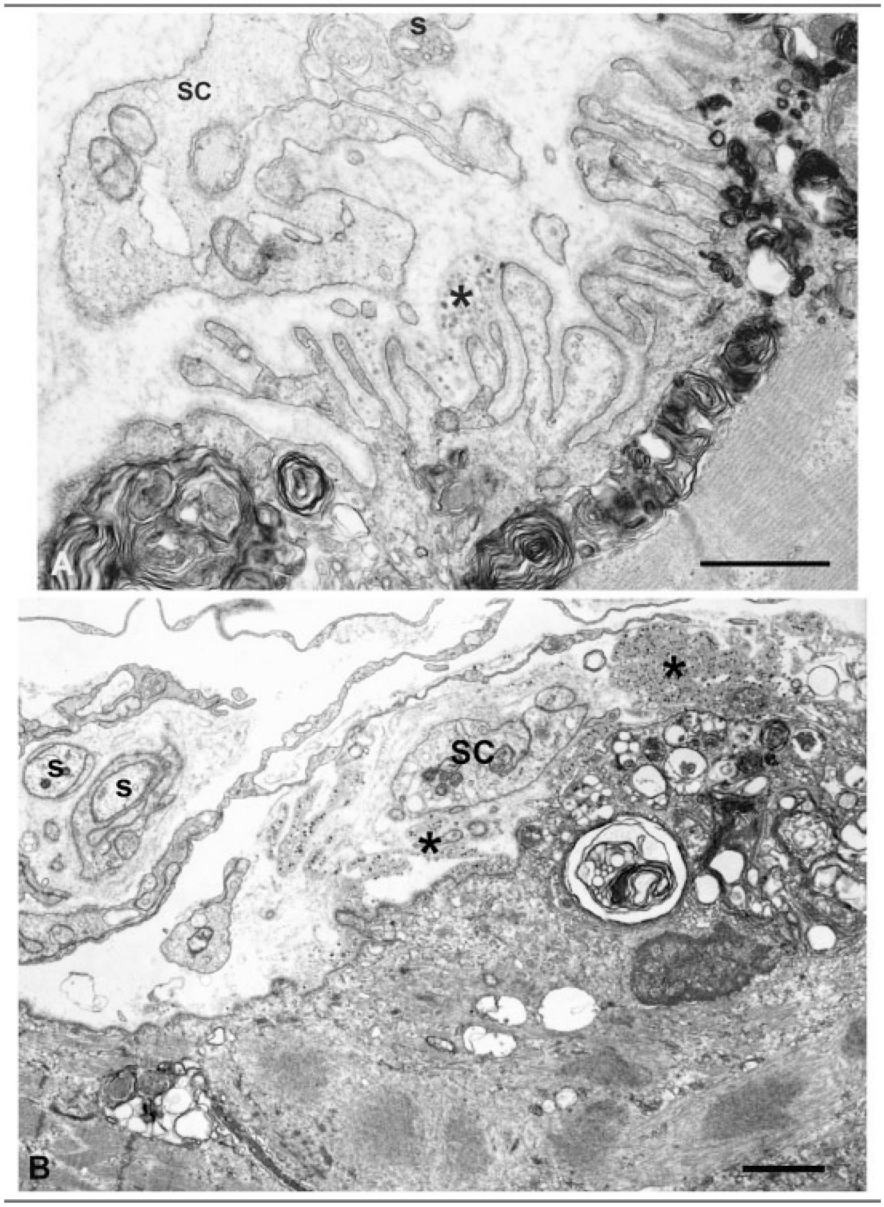

Fig 5.

End plates (EPs) with presynaptic and postsynaptic abnormalities. (A) A highly abnormal EP region devoid of nerve terminal. Some junctional folds are degenerating (asterisk). The subsynaptic sarcoplasm harbors large myeloid structures. Nerve sprouts (s) surrounded by Schwann cell (SC) appear above the junction. EP region in (B) is denuded of its nerve terminal and shows marked degeneration of its junctional folds (asterisks) and subsynaptic organelles. Schwann cell process (SC) is present amid relics of the folds. Two nerve sprouts (s) appear at top left. Bars = 1μm.

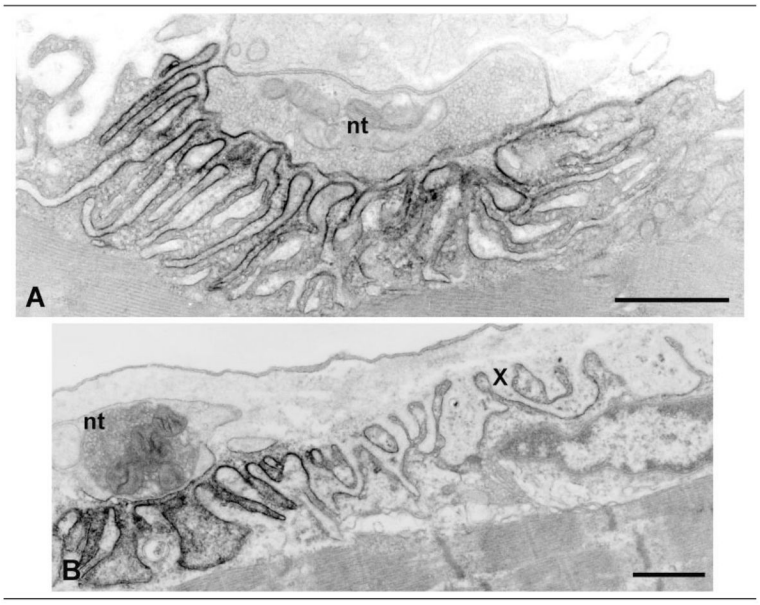

Fig 6.

Acetylcholine receptor (AChR) localization with peroxidase-labeled α-bungarotoxin (α-bgt). (A) Junctional folds are preserved and show a normal density and distribution of AChR. (B) Folds at bottom left react strongly for AChR but are capped by a degenerating nerve terminal. The folds at top right are degenerate, do not react for AChR, and are not covered by nerve terminal. nt = nerve terminal. Bars = 1μm.

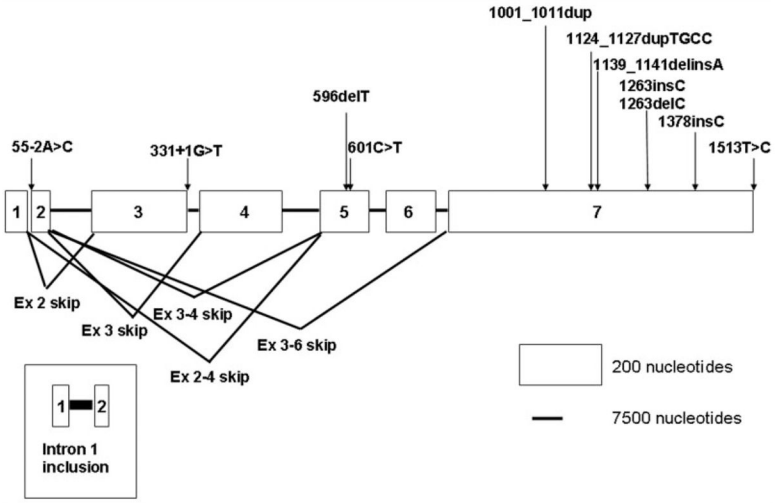

Fig 7.

Genomic structure of DOK7 and identified rearrangements in 16 patients. (inset) Intron 1 retention *(thick horizontal line).*

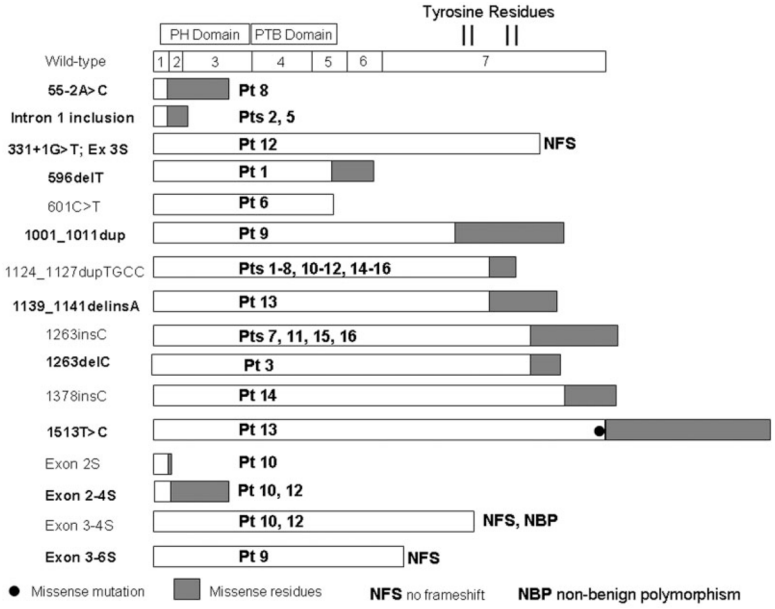

Fig 8.

Scaled linear models of wild-type DOK7 and predicted peptides of mutant transcripts. White and shaded regions represent wild-type and missense residues. *Solid circle* shows location of missense mutation. The pleckstrin homology (PH) and phosphotyrosine-binding (PTB) domains, and the four important tyrosine residues in exon 7 are marked in wild type. Novel rearrangements are indicated in boldface type. NFS = no frameshift; NBP = nonbenign polymorphism.

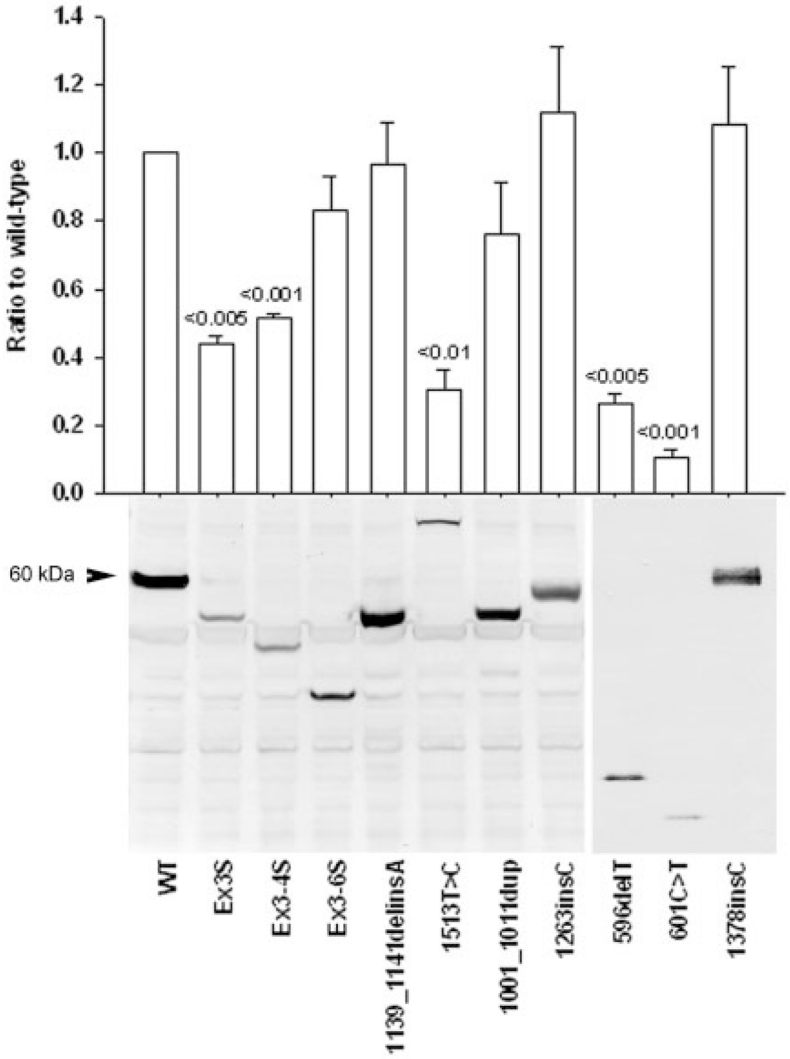

Fig 9.

Immunoblot demonstrating expression of wild-type (WT) and mutant DOK7 transcripts in human embryonic kidney (HEK) cells. Expression levels are normalized for cotransfected β-galactosidase. Bars indicate means and standard errors of four transfections.

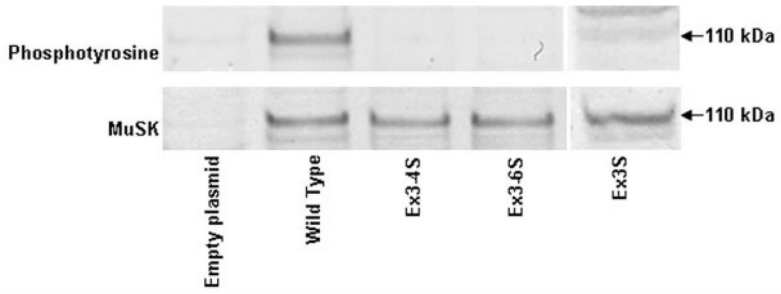

Fig 10.

Immunoblot demonstrating MuSK and phosphorylated MuSK in affinity-purified extracts of human embryonic kidney (HEK) cells transfected with MUSK and wild-type or exon-skipped constructs of DOK7. Products of transcripts lacking exons 3, 3 to 4, or 3 to 6 do not phosphorylate MuSK.

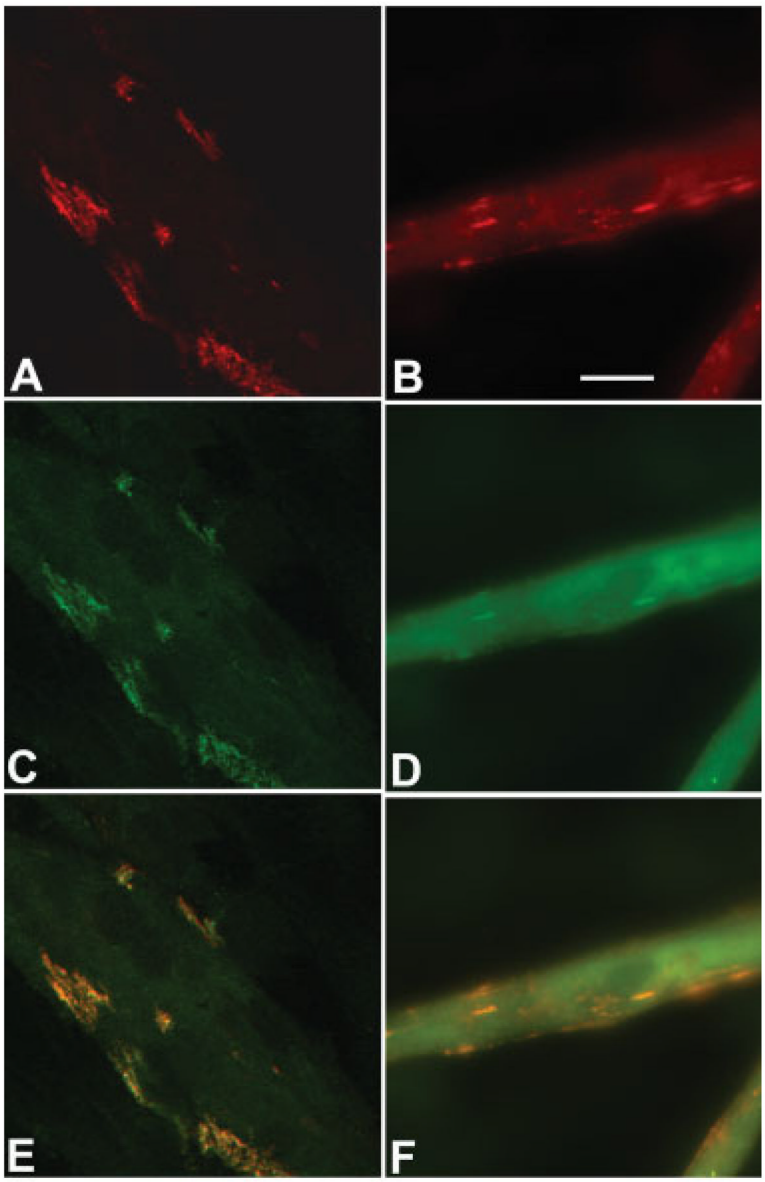

Fig 11.

Localization of acetylcholine receptor (AChR; red; A, B), Flag-Dok-7 (green; C, D), merge (E, F) in C2C12 myotubes transfected with Flag-tagged wild-type (A, C, E) and flag-tagged 1139_1141delinsA-DOK7 complementary DNA (B, D, F). Apotome optics, 0.43μm slice distance. Scale bar = 20μm.

Table 1

Clinical Features in 16 Patients

Clinical Features	Affected Patients (n)
Decreased fetal movements	3
Onset in neonatal period or early infancy	10
Fatigable weakness	16
Proximal limb weakness	16
Proximal and distal limb and axial weakness	5
Eyelid ptosis (asymmetric in some patients)	14[a]
Oculoparesis	6[b]
Facial weakness	13[c]
Bulbar symptoms	11
Respiratory symptoms	13[d]
Documented abnormal pulmonary function tests	7
Intermittent worsenings	10[e]
Progressive course	12
Electromyographic decrement in some muscles	16[f]

[a] Mild in eight, moderate in five, and severe in one patient.

[b] Mild in five and moderate in one patient.

[c] Mild in eight and moderate in five patients.

[d] Two patients had ventilatory failure at birth but improved during infancy.

[e] Lasting few days to few weeks.

[f] Not present in all muscles; typically maximal in trapezius.

Table 2

Frequencies (%) of Conformational Changes at End Plates in Patients and Control Subjects

Conformational Changes	Patients	Control Subjects
Degenerating junctional folds[a]	33	4
Partially occupied postsynaptic region	19	0
Denuded postsynaptic region	18	9
Absent or highly simplified junctional folds[b]	16	9
Degenerating subsynaptic organelles	10	0
Schwann cell encasement of nerve terminals	9	0
Degenerating nerve terminals	3	0

A total of 613 Dok-7 and 162 control end-plate (EP) regions were analyzed. An EP region is defined as a nerve terminal and the associated postsynaptic region. More than one region can occur at an EP, and more than one conformational change can occur at an EP region.

[a] Degeneration of junctional folds also simplifies the postsynaptic region.

[b] Exclusive of postsynaptic regions with degenerating junctional folds.

Table 3

Morphometric Analysis of End-Plate Regions

End-Plate Regions	Patients (number of patients; number of regions)	13 Control Subjects (number of regions)	*p*
Mean nerve terminal area ± SE, μm^2	3.43 ± 0.16 (14; 340)	3.88 ± 0.39 (63)	NS
Mean postsynaptic area ± SE, μm^2	6.69 ± 0.21 (14; 340)	10.60 ± 0.79 (59)	<0.001
Mean postsynaptic membrane length/ postsynaptic area ± SE, $\mu m/\mu m^2$	3.93 ± 0.07 (14; 340)	5.83 ± 0.25 (47)	<0.001
Mean postsynaptic membrane length/ primary synaptic cleft length ± SE, $\mu m/\mu m^2$	6.82 ± 0.23 (14; 340)	10.10 ± 0.75 (39)	<0.001
Mean AChR index ± SE[a]	2.43 ± 0.18 (12; 154)	3.01 ± 0.09 (85)	<0.005

More than one region can occur at an end plate (EP).

[a] Acetylcholine receptor (AChR)–reactive postsynaptic membrane length normalized for the length of the primary synaptic cleft. SE ± standard error; NS = not significant.

Table 4

Microelectrode Studies of Neuromuscular Transmission and [^{125}I]α-Bungarotoxin Binding Sites per End Plate

Mean ± SE	Patients (n)	Control Subjects (n)	*p*
EPP quantal content, m[a]	25 ± 2.2 (14)	30 ± 2.0 (15)	NS
$MEPP_A$ amplitude, mV[b]	0.66 ± 0.05 (14)	0.99 ± 0.07 (15)	0.011
Predicted EPP, mV ($m \times MEPP_A$)	16.0 ± 1.5 (14)	28 ± 1.5 (15)	<0.011
MEPC amplitude, nA[c]	3.2 ± 0.22 (12)	3.9 ± 0.15 (10)	0.018
Single-channel opening bursts, milliseconds[d]	3.42 ± 0.16 (7)	3.0 ± 0.26 (7)	NS
[^{125}I]α-bungarotoxin binding sites/EP	6.52 ± 0.9 E6 (12)	12.82 ± 0.79 E6 (13)	0.011

Intracellular recordings were with beveled 10 to 20MΩ electrodes; patch-clamp recordings were with 5 to 10MΩ fire-polished Sylgard-coated borosilicate glass electrodes.

[a] Quantal content of end-plate potential (EPP) at 1Hz stimulation corrected for resting membrane potential of −80mV, nonlinear summation, and non-Poisson release. Temperature = 22 ± 0.5°C.

[b] Corrected for resting membrane potential of −80mV and a mean muscle fiber diameter of 50μm; temperature = 22 ± 0.5°C.

[c] −80mV; temperature = 29 ± 0.5°C.

[d] Acetylcholine level = 1μM; bandwidth, 5.8kHz for patients and 12kHz for control subjects; membrane potential = −80mV. $MEPP_A$ = amplitude of the miniature end-plate potential; NS = not significant; MEPC = miniature end-plate current.

Table 5

Rearrangements in DOK7 Observed in 16 Patients

Patients	Complementary DNA	Protein
1	596delT	Ile199ThrfsX47
	1124_1127dupTGCC	Ala378SerfsX30
2	Intron 1 inclusion[a]	Tyr19ValfsX23
	1124_1127dupTGCC	Ala378SerfsX30
3	1263delC	Ser422HisfsX34
	1124_1127dupTGCC	Ala378SerfsX30
4	1124_1127dupTGCC	Ala378SerfsX30
	1124_1127dupTGCC	Ala378SerfsX30
5	Intron 1 inclusion[a]	Tyr19ValfsX23
	1124_1127dupTGCC	Ala378SerfsX30
6	601C>T	Arg201X
	1124_1127dupTGCC	Ala378SerfsX30
7	1263insC	Ser422LeufsX97
	1124_1127dupTGCC	Ala378SerfsX30
8	55-2A>C (IVS1-2A>C)	Trp19ValfsX70
	1124_1127dupTGCC	Ala378SerfsX30
9	1001_1011dup	Ser338AlafsX122
	101_652del	Ex3-6 skipping
10	55_100del[b]	Ex2 skipping
	1124_1127dupTGCC	Ala378SerfsX30
11	1263insC	Ser422LeufsX97
	1124_1127dupTGCC	Ala378SerfsX30
12	331+1G>T (IVS3+1G>T)[b]	Ex3 skipping
	1124_1127dupTGCC	Ala378SerfsX30
13	1139_1141delinsA	Ala380AspfsX76
	1513T>C	X505Argext183
14	1378insC	Gln460ProfsX59
	1124_1127dupTGCC	Ala378SerfsX30
15	1263insC	Ser422LeufsX97
	1124_1127dupTGCC	Ala378SerfsX30
16	1263insC	Ser422LeufsX97
	1124_1127dupTGCC	Ala378SerfsX30

[a] Included intron carries a 15-nucleotide deletion.

[b] Cloned complementary DNA of Patients 10 and 12 showed multiple transcripts.